Harmonics Mitigation and Non-Ideal Voltage Compensation Utilizing Active Power Filter Based On Predictive Current Control

Alhasheem, Mohammed Adel Mohammed Zaki Youssef; Mattavelli, Paolo; Davari, Pooya

Published in:
IET Power Electronics

DOI (link to publication from Publisher):
10.1049/iet-pel.2019.0985

Publication date:
2020

Document Version
Accepted author manuscript, peer reviewed version

Harmonics Mitigation and Non-Ideal Voltage Compensation Utilizing Active Power Filter Based On Predictive Current Control

M. Alhasheem [1,2,*], *P. Mattavelli* [3], *P. Davari* [2]

[1] *Arab Academy for Science, Technology and Maritime Transport, 2033, Cairo, Egypt*
[2] *Energy Department, Aalborg university, Pontoppidanstraede 111, DK-9220 Aalborg East , Denmark*
[3] *Management and Engineering Department, University of Padua,Vicenza, Italy*
* *E-mail: m.a.hasheem@gmail.com*

Abstract: It is well-known that the presence of nonlinear loads in the distribution system can impair the power quality. Furthermore, the problem becomes worse in microgrids (MGs) and power electronic-based power systems as the increasing penetration of single-phase distributed generation may result in more unbalanced grid voltage. Shunt active power filters (SAPFs) are used for improving the power quality and compensating the unbalance grid voltage. This paper presents a modification of the classical control structure based on the finite control set model predictive control (FCS-MPC). The proposed control structure can retain all the advantages of finite control set MPC, while improving the input current quality. Furthermore, a computationally efficient cost function based on only a single objective is introduced, and its effect on reducing the current ripple is demonstrated. The presented solution provides a fast response to the transients and as well as it compensates for the unbalanced grid voltage conditions. A straightforward single loop controller is compared to the conventional way of realizing the APFs, which is based on space vector pulse width modulation (SVPWM). Moreover, the proposed control solution is compared with some of the control structures in the literature. The comparison has been done in terms of dynamic response, input current total harmonic distortion (THDi), and controller structure complexity. The simulation results have been obtained from MATLAB/SIMULINK environment, while the obtained experimental results, utilizing a 15 kVA power converter, highlight the effective performance of the proposed control scheme and verifies the introduced MPC based method as a viable control solution for SAPFs.

1 Introduction

The proliferation of nonlinear loads in the power electronic-based power system field has attracted the attention of researchers and industry to further prevent and protect the future power system from harmonic contamination. Generally, harmonics generated by nonlinear loads have caused many power quality problems. Not only, they cause power factor degradation, which impairs the performance of a power system, but they also cause other severe issues such as equipment overheating, measurement errors, failures of sensitive devices, and capacitor blowing. Therefore, it is mentioned in the different standards that the harmonics content should be below certain limits, and these limits can be defined based on the considered application. Conventionally, passive harmonic filters are employed in the filtering stages at the converter level or system level to deal directly with the harmonic issues. Due to their major weaknesses either in bulk sizes or fixed/limited mitigation abilities, an efficient harmonic mitigation technique, as shown in Fig. 1, known as active power filter (APF) is developed to replace the passive filters. Various studies have surveyed and reviewed APFs from different perspectives [1–5]. Some review studies categorized the APF operation based on the mitigation approaches, and some of them classified it based on the converter type, applied topology, control algorithms, and designed applications. In the same context, other studies have shown different configurations and all possible combinations of the basic power filters. In [5], a detailed review of different control algorithms of APFs is presented, where the current reference following techniques, dc-link voltage regulation, and instantaneous power are examined and discussed. While some control algorithms have more advantages over the others, they provide approximately the same performance in steady-state operations if the source voltage is ideal (not distorted or unbalanced). It is worth to notice that in [1, 6, 7] it is shown that not all the control algorithms are working appropriately in the presence of a non-ideal voltage. As discussed in [8–10], SAPFs are the most suitable to deal with harmonic current distortion as well as improving the total power factor performance by reducing the reactive power burden on the power system [11].

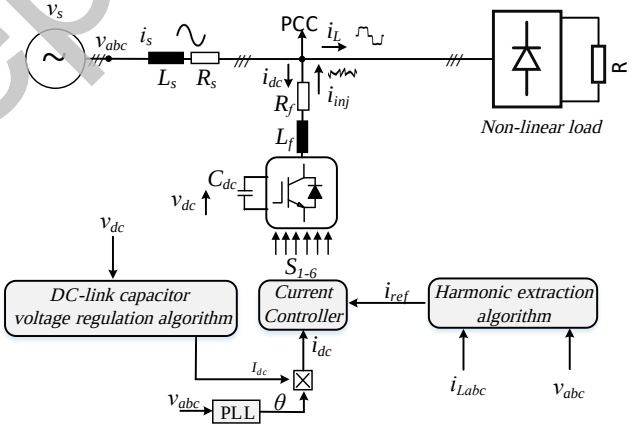

Fig. 1: General power circuit and current control structure of a shunt active power filter (SAPF).

However, the control of an active filter requires fast dynamic responses, and that represents a challenging control issue. Moreover, as a high control bandwidth is required, this leads to high sampling frequency requirement as well. On top of that, using the classical PI controllers may be hard to suppress the necessary supply disturbances [11]. In fact, proportional integrator (PI) controllers in a stationary reference frame failed to eliminate the steady-state error and to achieve satisfactory tracking performance of the desired reference [3]. PI and also proportional resonant (PR) controllers are sensitive to disturbances and need quite an effort, particularly in the case of the unbalanced grid, often by adding more controller blocks. As a result, tuning the controller becomes an extra burden. Moreover, the conventional deadbeat current control technique can provide a

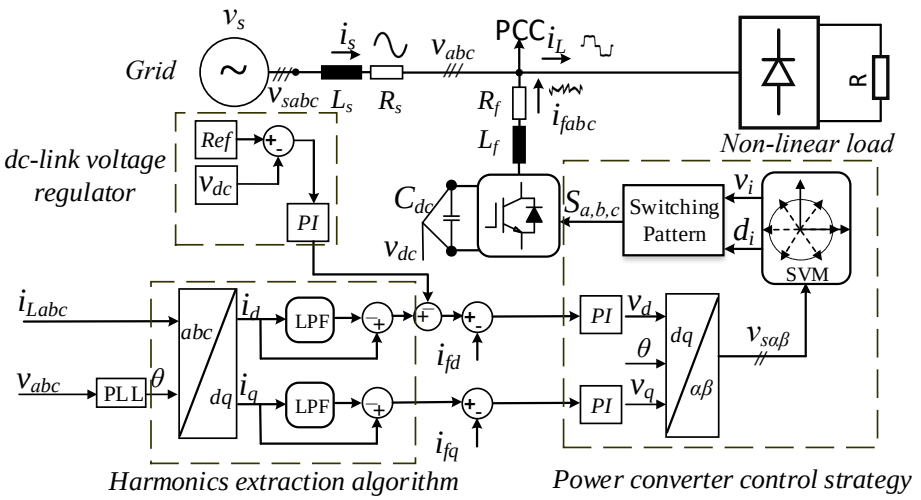

(a) Classical SVPWM.

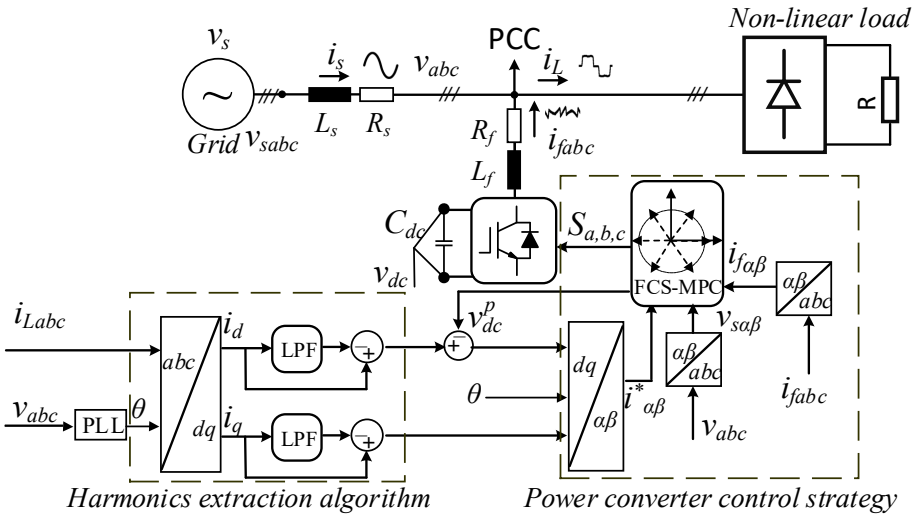

(b) Proposed FCS-MPC.

Fig. 2: Control structure showing the dc-link voltage regulation, harmonic extraction stage, PLL circuit, and current control strategy for the SAPF used in this work. (a) The conventional SVPWM; and (b) the proposed FCS-MPC control algorithm.

quite satisfactory dynamic performance when the converter load is exactly identified. Therefore, in [12] the analysis procedure reveals the stability and robustness margins of the algorithm considering its typical implementation. However, its dynamic performance has not been significantly promoted.

On the other hand, the unbalanced ac voltages have been considered to be one of the most significant challenges for the converters control to keep them normally operating and connected to the ac source [13, 14]. Several control algorithms have been proposed in order to regulate the negative and positive sequence currents and handle the unbalance problems [15, 16]. Some approaches have achieved low switching frequency, whereas some other methods obtain lower power ripples [17]. It is known that the unbalanced grid voltage causes an unacceptable percentage of oscillation in the power quantities [18, 19]. Hence, fundamentally, sequence extraction methods are required to improve power quality. However, most introduced methods focus on the control in the ideal/normal conditions without considering the unbalance grid or the severely unbalanced voltage. As a result, it is important to introduce a new control structure of the SAPF, which can compensate for the harmonics and unbalanced conditions. Besides, the proposed structure should be less sensitive to parameter variations and external disturbances. Therefore, FCS-MPC, as an intuitive control strategy, has good adaptability and robustness without inner current control loops and a modulator [20–23]. The prediction model is used to calculate the inverter behaviour at every sampling instant. Then, the optimal voltage vector is selected by a pre-programmed cost function (CF) and applied during the next sampling period [24, 25].

In this paper, a new control structure of a shunt active power filter (SAPF) based on FCS-MPC scheme is introduced to control a SAPF in MGs operations, as shown in Fig. 3, for compensating the harmonics and unbalanced grid voltages. In order to classify the proposed control performance, a conventional control structure has been implemented for the sake of comparison. The reference current of the SAPF is calculated using *dq* theory. The phase-locked loop (PLL) is adopted for generating the reference value of the compensation currents. A single-objective model predictive control method that deals with three main control targets is introduced. The control targets are to compensate unbalanced grid voltage, to compensate the reactive power and current harmonics, and to balance the dc capacitor voltage by using predefined ac currents. These targets are accomplished without spending tuning control efforts leading to avoid multiobjective optimization or empirical procedures for weighting factors determination. Thereby, the method is easy to implement and rapidly selects the optimal switching states to improve the dynamic-state performance of the SAPF. Also, the proposed control structure is

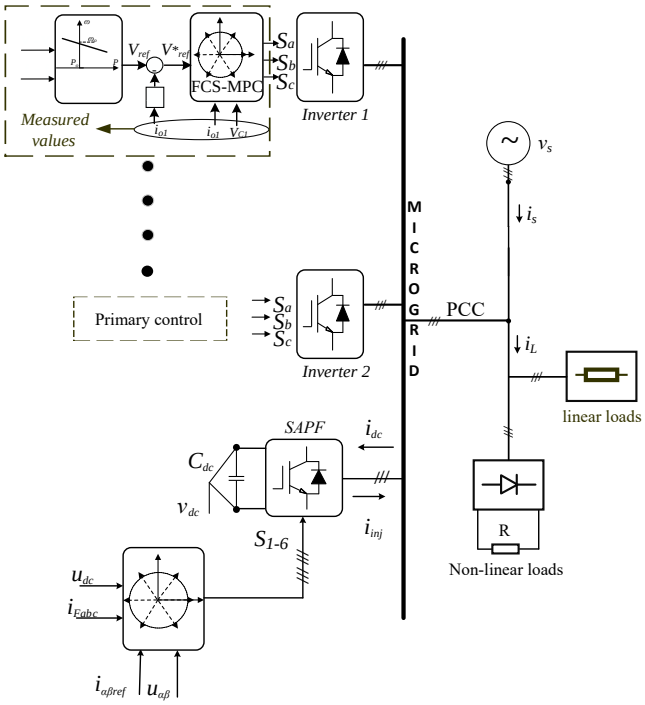

Fig. 3: The studied microgrid structure.

compared to some of the reported control structures in [26] and they have almost similar parameters to the proposal in this work. Contributions and novelty of this research are briefly presented as follows:

☐ The proposed current control provide a high control bandwidth, allowing fast harmonics compensation. That also provides a high level of compatibility since the fundamental dq harmonic extraction theory is slower than the instantaneous pq theory and that introducing a better performance of a SAPF.

☐ For the dc-link voltage regulation, the proposed control structure obtains the dc-link voltage based on the ac currents. Then use the obtained value in regulating the dc voltage without the need of the PI regulator, allowing for a simplicity in the implementation and fast dc voltage restoration.

☐ The proposed current controller is based on a single objective cost function resulting in avoiding the tuning control effort.

The remainder of the paper is structured as follows: the control structure of a shunt active power filter is described in Section 2. In Section 3, a conventional control structure method is explained and discussed. The system description and the proposed controller are described in Section 4. In Section 5, the obtained results and remarks are given. Finally, a summary of the work is presented in Section 6.

2 Control Structure of a Shunt Active Power Filter

In Fig.1, the overall circuit configuration of a SAPF is shown. It illustrates the main control stages. Generally, a shunt active power filter is connected to a harmonic producing power system at the point of common coupling (PCC), which is located between the harmonics producer load and the voltage supply. The basic active power filter system structure consists of four control stages, namely, harmonics extraction, dc-link voltage regulation, power converter control, and a synchronizer. In [5, 11], detailed explanation of the basic forms of the four control stages is provided. a SAPF controller determines in real-time the compensating current reference and forces the power converter to synthesize it as accurately as possible. Harmonics extraction stage separates the fundamental and oscillation components in order to inject the opposition of the currents exactly in phase with those are drawn by the non-linear load. By compensating the harmonics in this way, SAPFs can compensate for the harmonic current of a selected nonlinear load and continuously track the change in its harmonic contents. In this paper, the compensation of the selected harmonic loads current will be taken into consideration as it is assumed that the distortion level of the voltage supply is low. A proper actuation is given to the power converter based on the tracked reference and it should be switched at the highest possible frequencies with a minimum dissipation of power. Normally $f_{sw} \gg f_{hmax}$, where f_{hmax} represents the frequency of the highest order of harmonics current. That is provided by the current control algorithm which is a vital part to obtain fast and high filtering ability. On the dc side, the active filter is connected to a capacitor in order to ensure a storage capability. It is required to maintain the dc-link voltage at its initial value continuously in order to provide reactive power compensation.

3 Shunt Active Power Filter Based on SVPWM

Conventionally, the control structure of a SAPF is based on measuring the nonlinear currents and grid voltages, which are measured in abc frame. Then, the phase angle (θ) is calculated using a conventional PLL circuit to transform the nonlinear load currents into the dq components, as calculated in (1) and (2). A high pass filter (HPF), which is implemented by the mean of HPF= 1-LPF, is used in this stage to separate the average and oscillatory dq components. The oscillatory dq components are filtered and they are compared with the actually measured filter currents i_f. As it can be seen from Fig. 2(a), a PI controller is functioning in order to regulate the dc-link voltage.

Furthermore, PI controllers are regulating the dq voltage components. SVPWM control strategy is based on the fact that the VSC possible switching states are finite. The two-level three-phase VSC has six active and two zero space (or voltage) vectors. The six active vectors produce a nonzero output voltage, and the two zero vectors produce zero output voltage. Space vector of the three-phase quantities is represented as vectors in a two-dimensional $\alpha\beta$ plan, as shown in Fig. 4. So, the concept of SVPWM technique is to use the reference voltage vector to identify the sector and calculate the switching time of the pulses. Firstly, it calculates the magnitude and the angle of the reference voltage vector. Then the switching time duration of each sector is calculated. Subsequently, the switching signals are calculated in order to compare them with the carrier. A comparison between the signals and the carrier is used to generate the IGBTs pulses. On the other hand, the unbalanced grid voltage compensation is achieved by a conventional positive and negative control strategy, which will be shown in Section 6.

$$\begin{bmatrix} v_d \\ v_q \end{bmatrix} = \begin{bmatrix} \cos(\theta) & \sin(\theta) \\ -\sin(\theta) & \cos(\theta) \end{bmatrix} \begin{bmatrix} v_\alpha \\ v_\beta \end{bmatrix} \quad (1)$$

$$\begin{bmatrix} v_\alpha \\ v_\beta \end{bmatrix} = \frac{2}{3} \begin{bmatrix} 1 & -\frac{1}{2} & -\frac{1}{2} \\ 0 & \frac{\sqrt{3}}{2} & -\frac{\sqrt{3}}{2} \end{bmatrix} \begin{bmatrix} v_a \\ v_b \\ v_c \end{bmatrix} \quad (2)$$

4 Proposed Control Structure and System Description

SAPF can produce any set of balanced currents to compensate the reactive power and current harmonics drawn by the nonlinear load. The power rating of the converter should be selected appropriately, as well as the controller bandwidth. Single-phase connectivity of the renewable sources results in unbalanced source voltage conditions (UbSVC). Furthermore, interfacing power electronic devices also inject the harmonics into the PCC voltage. Therefore, the presence of voltage unbalances, and harmonics can adversely affect the DGs

as well as the power system in the MG applications. Compensator devices [4, 8], such as APF [27], can compensate for these abnormal conditions and enhance the power quality in order to meet the grid requirements. Many control structures and algorithms are proposed and evaluated as in [11, 28]. Some methods, like discussed in [10, 29], introduced a dq control frame. Other ways, as described in [2, 30], are proposing the pq theory for the harmonics extraction mechanism. Each method has its pros and cons, as presented in [11, 29, 31]. Moreover, several works have discussed the power converter controller, as presented in [2–4, 9, 20, 32]. The new control structure in this paper is utilizing the predictive control and compare it with a similar structure using the space vector control as explained in the previous section. As shown in Fig. 2(b), the harmonic extraction stage has a PLL circuit, which is used to calculate the phase angle of the grid voltage. The calculated phase angle is used to obtain the dq components of the non-linear load current. A low pass filter is designed to separate the average and oscillatory components of the i_d and i_q as follows:

$$\begin{aligned} i_d &= \bar{i_d} + \widetilde{i_d} \\ i_q &= \bar{i_q} + \widetilde{i_q} \end{aligned} \tag{3}$$

Where $\bar{i_{dq}}$ are the average values and $\widetilde{i_{dq}}$ are the oscillatory parts. The utilized LPF is designed with a cut-off frequency of 25 Hz and quality factor [(Q) = 0.707]. The filter parameters selection is based on a compromise between fast dynamic response and acceptable filtering performance. Due to the absence of a modulator, the only possible control actions are the ones generated by the eight possible inverter switching states:

$$S(k) = \left\{ \begin{bmatrix}0\\0\\0\end{bmatrix} \begin{bmatrix}0\\0\\1\end{bmatrix} \begin{bmatrix}0\\1\\0\end{bmatrix} \begin{bmatrix}0\\1\\1\end{bmatrix} \begin{bmatrix}1\\0\\0\end{bmatrix} \begin{bmatrix}1\\0\\1\end{bmatrix} \begin{bmatrix}1\\1\\0\end{bmatrix} \begin{bmatrix}1\\1\\1\end{bmatrix} \right\} \tag{4}$$

The shunt active filter currents equations can be expressed as:

$$\frac{\mathrm{d}i_{f_\alpha}}{\mathrm{d}t} = \frac{1}{\mathrm{L_f}} v_{s\alpha}(t) + \left(1 - \frac{\mathrm{R_f}}{\mathrm{L_f}}\right) i_{f_\alpha}(t) - \frac{1}{3\mathrm{L_f}} N_1[S(t)] v_{dc} \tag{5}$$

$$\frac{\mathrm{d}i_{f_\beta}}{\mathrm{d}t} = \frac{1}{\mathrm{L_f}} v_{s\beta}(t) + \left(1 - \frac{\mathrm{R_f}}{\mathrm{L_f}}\right) i_{f_\beta}(t) - \frac{1}{3\mathrm{L_f}} N_2[S(t)] v_{dc} \tag{6}$$

where L_f and R_f are the filter inductor and equivalent resistor and

$$\begin{aligned} i_{s\alpha}(t) &= i_{l\alpha}(t) + i_{f\alpha}(t) \\ i_{s\beta}(t) &= i_{l\beta}(t) + i_{f\beta}(t) \end{aligned} \tag{7}$$

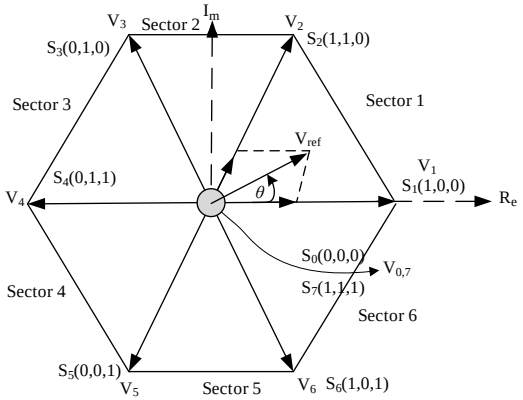

Fig. 4: Space vector diagram and the voltage vectors generated by the inverter (V_i).

At the k^{th} time instant the controller uses (8, 9) to predict the future system state value for each possible control action in (10).

$$i_\alpha^p\left(k+1\right) = \frac{\mathrm{T_s}}{\mathrm{L_f}} v_{s_\alpha}(k) - \frac{\mathrm{R_f T_s}}{\mathrm{L_f}} i_{f_\alpha}(k) - \frac{\mathrm{T_s}}{3\mathrm{L_f}} N_2[S(k)] v_{dc} \tag{8}$$

$$i_\beta^p\left(k+1\right) = \frac{\mathrm{T_s}}{\mathrm{L_f}} v_{s_\beta}(k) - \frac{\mathrm{R_f T_s}}{\mathrm{L_f}} i_{f_\beta}(k) - \frac{\mathrm{T_s}}{3\mathrm{L_f}} N_2[S(k)] v_{dc} \tag{9}$$

$v_{\alpha\beta}$ are the grid voltages, v_{dc} is the dc-link voltage, $N_1 = [2 \quad -1 \quad -1]$ and $N_2 = [-1 \quad 2 \quad -1]$

$$S(k) = \begin{bmatrix} S_a(k) & S_b(k) & S_c(k) \end{bmatrix}^T. \tag{10}$$

Conventionally, in order to maintain the dc-link at the desired voltage, a PI controller is embedded in the control structure for dc-link voltage regulation. In this work, the dc-link voltage is predicted based on the ac currents and at the k^{th} instant will be written as follows:

$$v_{dc}^p\left(k+1\right) = v_{dc}(k) + \frac{\mathrm{T_s}}{\mathrm{C_{dc}}} h_1 S(k) i_{f\alpha}(k) + \frac{\mathrm{T_s}}{\mathrm{C_{dc}}} h_2 S(k) i_{f\beta}(k). \tag{11}$$

Where $h_1 = [1 \quad 0 \quad -1]$, $h_2 = [0 \quad 1 \quad -1]$ and C_{dc} is the capacitor value. As the measured filter currents are in the stationary reference frame, the dq components of the new reference currents are transformed in the stationary reference frame. The predictive control algorithm is using a single cost function (CF) in order to predict the filter currents and evaluate the error as follows:

$$g = (i_{f\alpha}^* - i_{f\alpha}^p(k+1))^2 + (i_{f\beta}^* - i_{f\beta}^p(k+1))^2. \tag{12}$$

Where $i_{f\alpha\beta}^p(k+1)$ and $i_{f\alpha\beta}^*$ are the predicted and reference currents, respectively. Model predictive control strategies take advantage of the fact that finite number of possible switching states are associated with voltage source converter (VSC). These states are discrete, and the model of the system can be used in association with a discrete-time model of the load to predict the behaviour of the VSC. A selection criterion, the objective function, is defined as a selection of the optimal future variables corresponding to the optimal future switching state that minimizes the objective function, which is the filter current in this case. For each predicted sampling period, the output variables are measured and compared with the reference variables to minimize the error. Usually, the sampling period is chosen as a period in which the reference current does not change significantly. Therefore, the reference variable can be considered as a constant for that period.

In general, model predictive control can include several objectives in a single CF without embedding hierarchal control loops, which are introducing a filtering behaviour in the system. Take into consideration that the desired objectives should be controlled with weighting factors to determine the objective importance. These weightings require tuning process, and the controller performance will be based on the points of operation but the FCS-MPC is considered as a robust control against parameter variations. One of the main ideas in this work is to achieve similar and even better compensation performance without using so many objectives in the CF. In that way, the controller structure is distinguished by having simplicity, reliability, and flexibility. On the other hand, reference current generation under unbalanced grid voltage is a crucial issue. The proposed solution uses a positive and negative sequence detection strategy with the MPC control unit. The positive and negative detection strategy is based on Fourier theory. A Fourier analysis is first applied to the three input signals (v_a, v_b, v_c) and for a specified fundamental frequency, it evaluates the phasor values of the voltages. Then the transformation is applied to obtain the positive sequence, negative sequence, and zero sequences given as:

$$v_P = \frac{1}{3}(v_a + av_b + a^2 v_c)$$
$$v_N = \frac{1}{3}(v_a + a^2 v_b + av_c) \quad (13)$$
$$v_0 = \frac{1}{3}(v_a + v_b + v_c)$$

where v_a, v_b, v_c are the voltage phasors at a specified frequency and $a = e^{(j2\pi/3)}$. The measured grid voltages are decomposed into a positive and negative sequence. Then, the positive sequence voltage is controlled and given to the harmonics extraction unit. In that way, the supply current is balanced and with less harmonic distortion. Therefore, in order to validate the performance of the proposed control algorithm, up to 10% voltage unbalance has been considered [13].

5 Results and Discussion

The conventional and proposed control structures have been verified experimentally, where a 15 kVA rated power system has been built and connected to the grid for that purpose as it can be seen in Fig. 5. The power system has been used experimentally to investigate the actual performance of the proposed control strategy compared to the SVPWM strategy. The ac side is connected to the mains point at the common coupling (PCC) using a three-phase inductive filter, which has an equivalent series parameters of L_f = 5 mH and R_f = 0.4 Ω. A three-phase diode bridge rectifier connected to a resistive load has been used as a nonlinear load in order to create a distorted grid current using a standard three-phase 230 V_{rms} and 50 Hz grid frequency. Table 1 illustrates all the parameters used in the experimental test. The control system is composed of a dSpace (DS 1007) power dual-core 2 GHz processor board. The maximum achieved turn around time was around 16 μs. The dSpace A/D converter samples at a rate of 1 MS/s. Hence, the time required for a sampling of one channel is approximately 1 μs. Since the algorithm has a synchronized sampling and switching procedure, the computational delay of T_s is needed to be compensated [33]. In order to validate the effectiveness of the proposed structure, the algorithm has been tested and compared against the standard SVPWM. A sampling frequency of 50 kHz and 20 kHz have been used for the FCS-MPC and the SVPWM, respectively. A steady-state test under 53% of the full load and a transient test for a 33% to 53% load variation are shown in Fig. 6. As it can be seen from the simulation result in Fig. 6, experimental result in Fig. 7 and the spectrum analysis in Fig. 8, the current harmonic distortion caused by the presence of the nonlinear load is actively compensated using the filtering system. For MPC, the main current does not present particular harmonics concentration but it shows an average of 10 kHz switching frequency, which is not the case for SVPWM as shown in Fig. 9. That explains the high-frequency ripple, which is related to the variable switching frequency due to the absence of a PWM modulator.

Moreover, the results show a reduction of total harmonic distortion (THDi) from THD > 28% to THD < 3.6% at 8 kW, where the THD is calculated up to the 40^{th} harmonics. The capacitor voltage and load current variations are realized by stepping up and down the rectifier load from 33% to 53% of the full load and they are presented in Fig. 10 and Fig. 11. The waveforms of the reference and predicted currents in $\alpha\beta$ frame during the transient are reported in Fig. 12. It can be noticed that the SAPF takes about 15 ms time to reach steady-state condition, exhibiting very fast dynamics and accurate tracking performance. Also by looking in Fig. 10, the previous observation is validated and the dc-link voltage remains well regulated with a maximum ripple to 0.14% of its nominal value. This result validates the proposed solution and shows the viability of the FCS-MPC for SAPF control by employing a single compact control loop that regulates all system relevant quantities. On the other hand, similar tests were

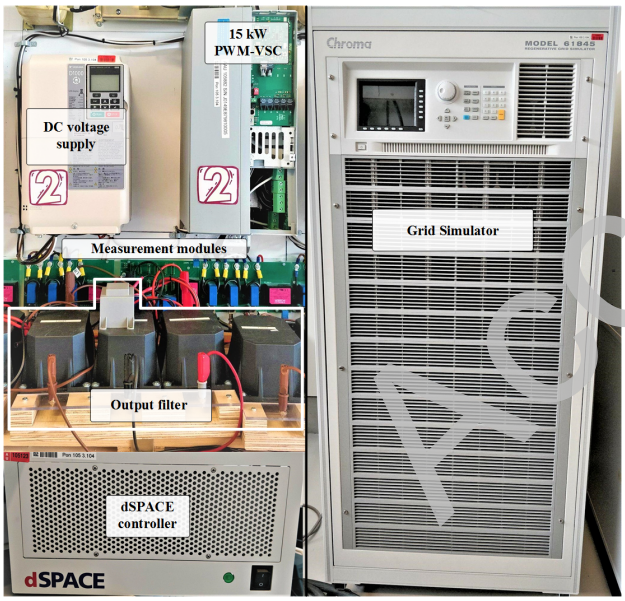

Fig. 5: Experimental setup.

Table 1 System Parameters for the Simulation and Experimental Setup.

Parameter	Quantity
S	15 kVA
V_o	400 V
V_{dc}	700 V
Grid frequency f_g	50 Hz
Switching frequency f_{sw} (SVM)	10 kHz
Switching frequency f_{sw} (MPC)	≈10 kHz
L_f	5 mH
Non-linear load	Diode rectifier and R = 60 Ω

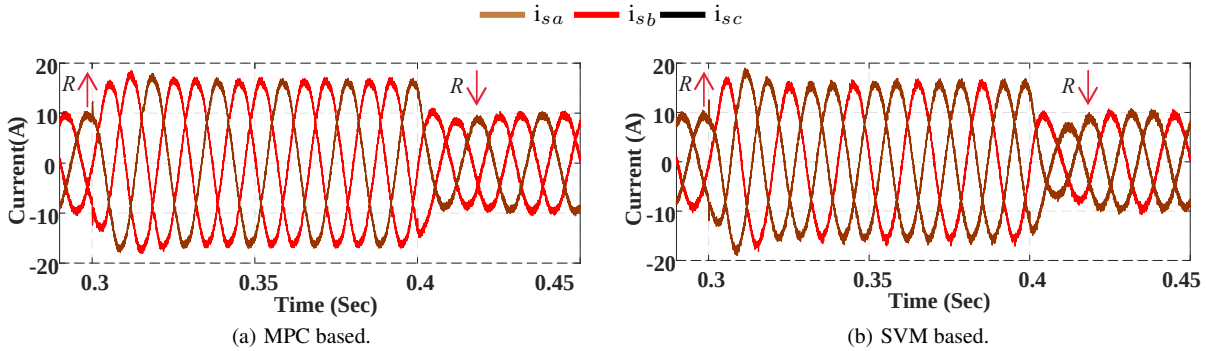

(a) MPC based. (b) SVM based.

Fig. 6: Simulated three-phase supply currents for both control algorithms, where the figures show the steady-state and transient operation from 33% to 53% step load and vice versa. (a) Supply currents using the proposed control structure; (b) supply currents using SVPWM.

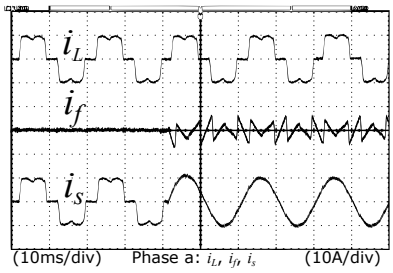

(a) Experimental result of the proposed FCS-MPC structure, where i_L is the non-linear load current measurements, i_f is filter current, and i_s grid current measurement.

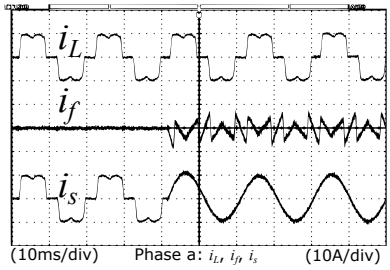

(b) Experimental result of the conventional SVPWM, where i_L is the non-linear load current measurements, i_f is the filter current, and i_s is the grid current measurement.

Fig. 7: Harmonics compensation. (a) Using the proposed control structure; and (b) using the conventional control structure.

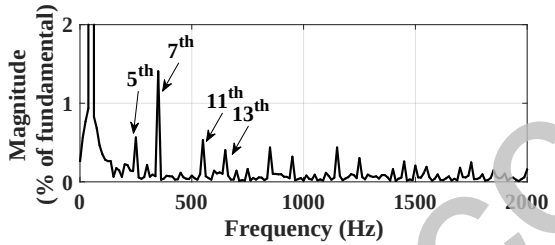

(a) Measured spectrum of (i_{sa}) using the proposed control structure.

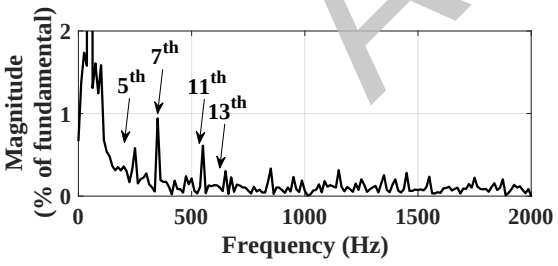

(b) Measured spectrum of (i_{sa}) using the conventional control structure.

Fig. 8: Frequency analysis of the compensated current (i_{sa}) in case of balanced grid voltage.

performed for the SVPWM to compare its performance with the proposed solution. Fig. 10 shows that the dynamic performance of the SVPWM during sudden load changes are qualitatively slower than the proposed MPC structure showing a 3.5 ms difference. Compared with the SVPWM, the proposed control technique presents a similar harmonic content (up to the 40th harmonic) for the mains current in the case of balanced grid voltage, as shown in Fig. 8. However, it

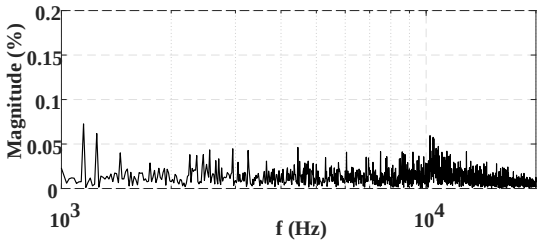

(a) The proposed MPC Spectrum

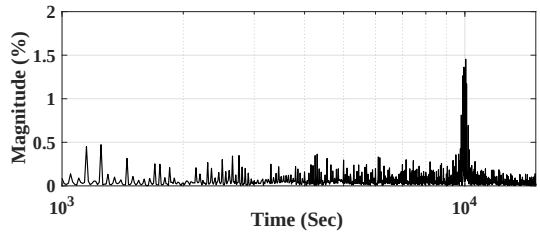

(b) SVPWM Spectrum

Fig. 9: Spectrum harmonics content of supply current i_s for both control structures. (a) Spectrum of the proposed MPC, while the calculated THDi = 3.6% at 8 kW and up to 2 kHz; and (b) spectrum of the classical SVPWM, while the calculated THDi = 4.3% at 8 kW and up to 2 kHz.

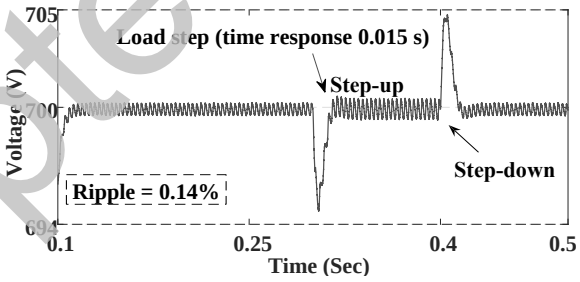

(a) Time response of the dc-link voltage using the proposed control structure for step up load change and similar step down load change.

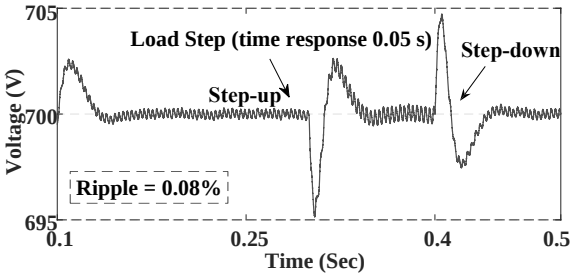

(b) Time response of the dc-link voltage using the conventional SVPWM structure for step up load change and similar step down load change.

Fig. 10: Capacitor voltage during the steady-state and transient operation for both controllers.

should be noticed that the sampling frequencies are different for the two controllers 20 kHz for the SVPWM and 50 kHz for the MPC, respectively. MPC requires a higher sampling frequency compared to the fixed switching frequency modulated approaches. Moreover, by increasing the MPC sampling frequency, a further mains current THD reduction is achievable. For dc-link voltage regulation, the PI controller for the dc-link voltage regulation is eliminated in the proposed MPC structure, and v_{dc} is obtained based on the ac converter currents.

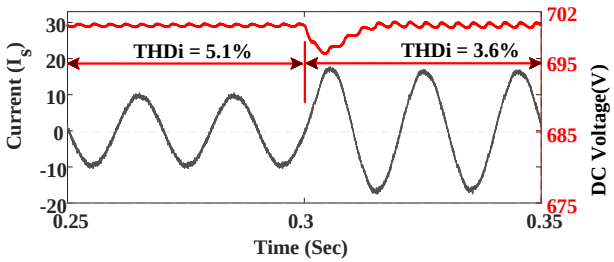

(a)

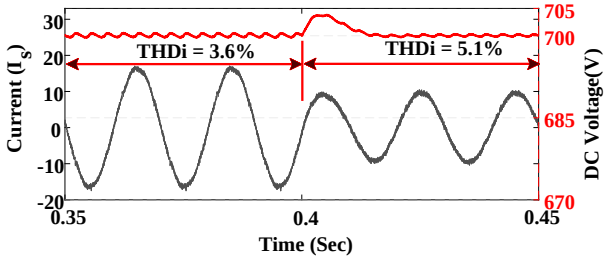

(b)

Fig. 11: Dynamic response of the dc-link voltage from 4 kW till 8 kW for the proposed control structure, where (a) dc-link voltage at a step up power from 4 kW to 8 kW; and (b) dc-link voltage at a step down power from 8 kW to 4 kW.

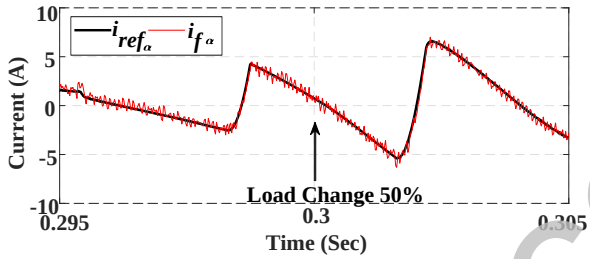

(a) Reference and injected currents (α currents)

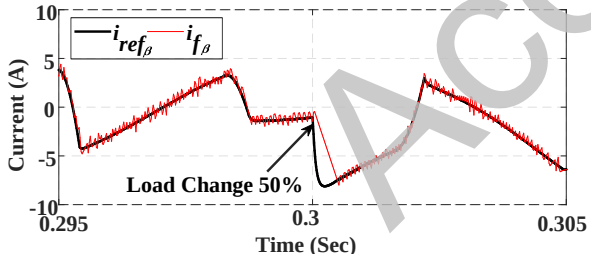

(b) Reference and injected currents (β currents)

Fig. 12: Dynamic response of the injected current (i_f) based on the reference current which is sent to the proposed controller. (a) Decoupled and injected current ($i_{f\alpha}$) to the grid for the compensation purposes; and (b) decoupled and injected current ($i_{f\beta}$) to the grid for compensation purposes.

Finally, using the proposed MPC control structure and the frequency domain sequence components detection allows the compensation of the unbalanced grid voltage. The proposed control structure does not use the conventional positive and negative control loop to decouple the dq components, as it can be seen in Fig. 13. The dq components are naturally decoupled by using the proposed FCS-MPC control structure after the transformation to a stationary reference frame and Fig. 12 presents this phenomenon. In Figs. 14, 15 and 16, comparative simulation results for voltage unbalance compensation are illustrated, where the amount of voltage unbalances has been calculated following IEC61000-2-2 in a three-phase

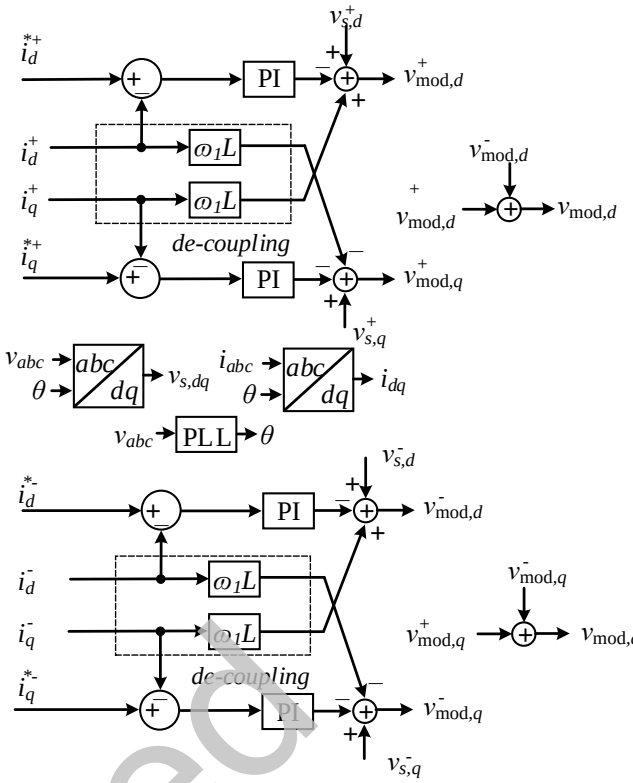

Fig. 13: Voltage unbalance compensation using positive and negative sequence controller used for classical SVPWM.

system as:

$$v_{unbalanced}(\%) = \sqrt{\frac{6 \times (v_{ab}^2 + v_{bc}^2 + v_{ca}^2)}{(v_{ab} + v_{bc} + v_{ca})^2} - 2} \qquad (14)$$

In order to compensate for the unbalanced grid voltage, supply currents (i_{sabc}) should be balanced. In the proposed control structure, the positive and negative sequence voltages are detected using the frequency-domain method, which is based on Fourier and the positive sequence voltage is controlled. In that way, the angle θ is correctly obtained and proceeded to the harmonics detection stage. Figs. 17, 18, and 19 show the spectrum of the proposed control structure and the conventional in case of 3%, 5% and 10% unbalanced grid voltages. The unbalance grid voltage compensation in the conventional control strategy, as mentioned before, is based on the positive control method, which is shown in Fig. 13. It can be seen easily which harmonic orders are suppressed compared to the spectrum in Fig. 20, which shows the spectrum of the load current while the SAPF is deactivated. Specifically, fifth and seventh harmonics show how the currents are distorted due to the presence of the non-linear load. Also, third harmonics are clearly observed due to the unbalanced grid voltage. The proposed control structure has the ability to suppress the third harmonics compared to the conventional controller. Both controllers were able to suppress the low harmonic components starting from the fifth order. As future work, selective harmonics order can be further suppressed by using other harmonic detection techniques such as the harmonics dq frame method. Fig. 21 shows and validates the performance of the proposed solution in compensating for the unbalanced grid voltage. THD$_i$ of each case at 6 A rated current is reported in Table 2. It also shows a comparison between the proposed control structure and other reported control methods in [26]. The conducted tests and parameters in that work are almost matching the conducted tests and parameters in this work. Thereby, it was interesting to show the performance of those methods with respect to the methods investigated in this work allowing to do a fair comparison.

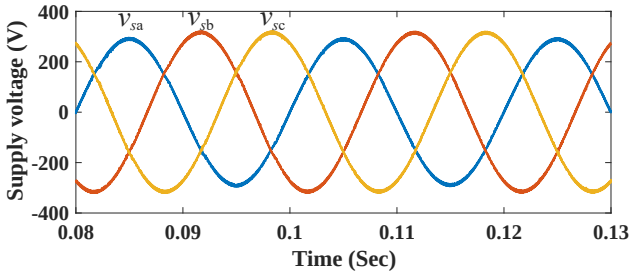

(a) 3% grid voltage unbalance (v_{sa}) following IEC 61000-2-2.

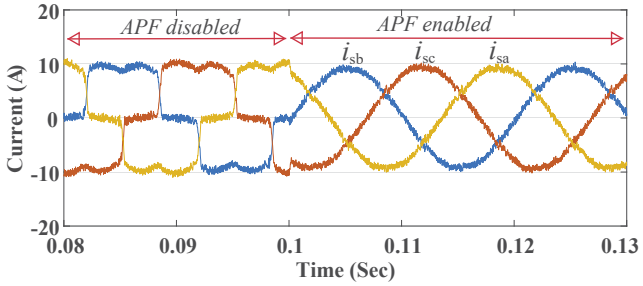

(b) Calculated THDi for phase a = 5.16%.

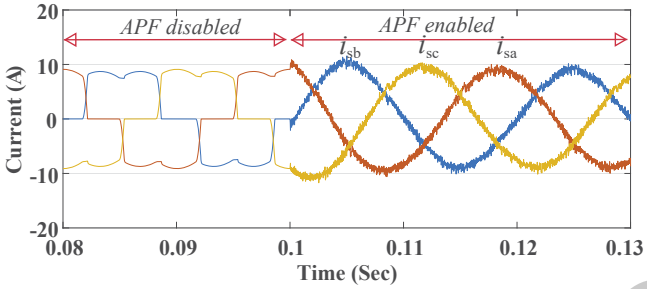

(c) Calculated THDi for phase a = 6.49%.

Fig. 14: Simulation results: harmonics and unbalance compensation using the proposed and classical control structure. (a) 3% grid voltage unbalance; (b) compensation in case of grid voltage unbalance using FCS-MPC, and (c) compensation in case of grid voltage unbalance using classical SVPWM.

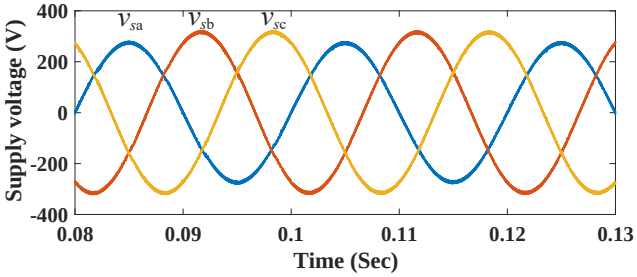

(a) 5% grid voltage unbalance (v_{sa}) following IEC 61000-2-2.

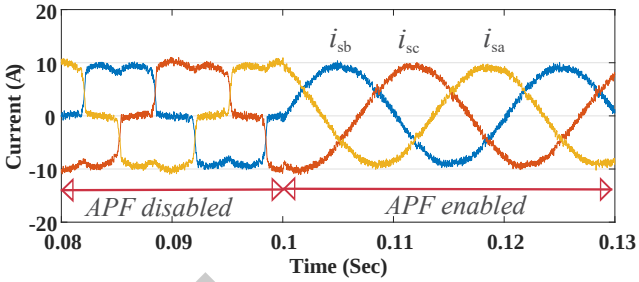

(b) Calculated THDi for phase a = 5.7%.

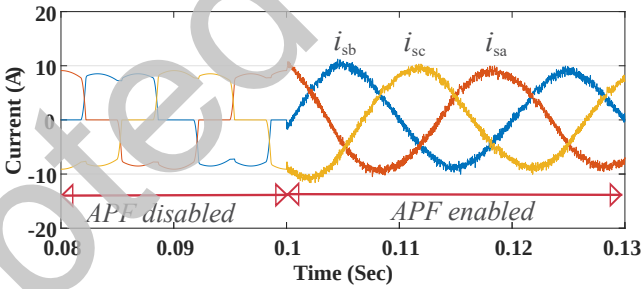

(c) Calculated THDi for phase a = 6.91%.

Fig. 15: Simulation results: harmonics and unbalance compensation using the proposed and classical control structure. (a) 5% grid voltage unbalance; (b) compensation in case of grid voltage unbalance using FCS-MPC, and (c) compensation in case of grid voltage unbalance using classical SVPWM.

In the end, the purpose of this study is to investigate the performance of the FCS-MPC in SAPF applications. To the best of our knowledge, the previous studies have addressed the performance of the FCS-MPC using pq method as in [26], where the system was controlled by several constraints in the cost function. As a result, a high computational burden was obtained. None of the previous studies has investigated the unbalance conditions up to 10% based on FCS-MPC and using dq reference frame. By looking into the cost function in this work, which is using the filter current (i_f), as the only constraint, to generate the optimum switching signals, it is clear that no need to weighting factor design stage and that ensures simplicity and robust design. It is worth to mention that the proposed controller in this work was intentionally subjected to the same operating conditions using the conventional SVM controller. The reason behind that is to show the effectiveness of the FCS-MPC in case of employing it instead of the existing conventional controllers. As it can be seen from Table 2, the proposed controller showed a slight improvement in terms of THDi compared to classical methods. The proposed FCS-MPC scheme has shown very fast restoration time when a step load of around 3 kW has been considered. Besides, the DC voltage has shown ripple less than the other schemes. The switching frequency has been concentrated around 10 kHz for SVM and approximately 10 kHz average for the proposed FCS-MPC controller. This condition is helpful in case of considering the losses evaluation.

6 Conclusion

Unbalances and reduced power quality are relevant topics in modern electrical networks. Therefore, the use of active filters becomes important for the reduction of harmonic distortions and unbalance voltage compensation in the power grids. In this paper, the development and the implementation of a SAPF regulated by a predictive controller for harmonic distortion reduction and unbalance compensation are presented. Based on the system model, the controller predicts dynamically the values of the variable of interest in order to obtain a control target optimization by minimizing a pre-defined cost function. Furthermore, the current ripples of the proposed MPC structure are meeting the grid requirements with fast dynamic performance. The proposed control structure eliminated the dc-link regulation loop by predicting the dc voltage based on the ac converter currents. The suggested method gave simplicity to the overall control structure. On top of that, the proposed control structure showed excellent results in compensating the unbalanced grid voltage. The experimental and simulation results showed the validity and effectiveness of the proposed control structure compared to the conventional SVPWM strategy. Also, it showed that the power filter, MPC based, can achieve comparable results using a single cost function with a sole objective and without any tuning process. In future work, obtaining a fixed switching frequency will be investigated by redesigning the cost function and its simplicity will be maintained.

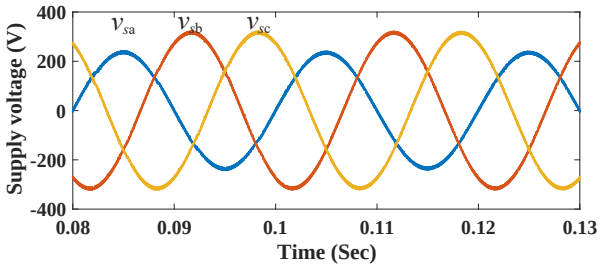

(a) 10% grid voltage unbalance (v_{sa}) following IEC 61000-2-2.

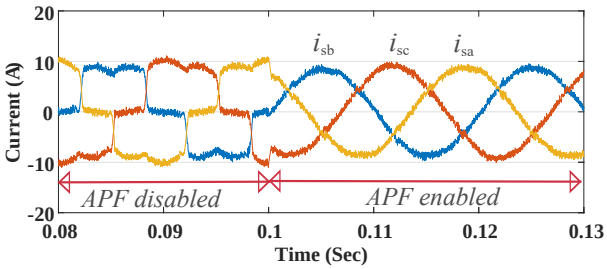

(b) Calculated THDi for phase a = 6.11%.

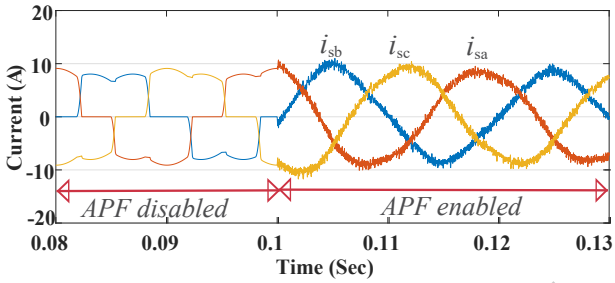

(c) Calculated THDi for phase a = 8.63%.

Fig. 16: Simulation results: harmonics and unbalance compensation using the proposed and classical control structure. (a) 10% grid voltage unbalance; (b) compensation in case of grid voltage unbalance using FCS-MPC, and (c) compensation in case of grid voltage unbalance using classical SVPWM.

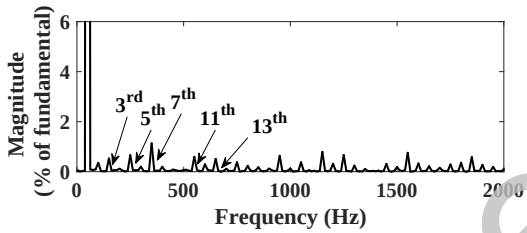

(a) Measured spectrum of (i_{sa}) using the proposed control structure.

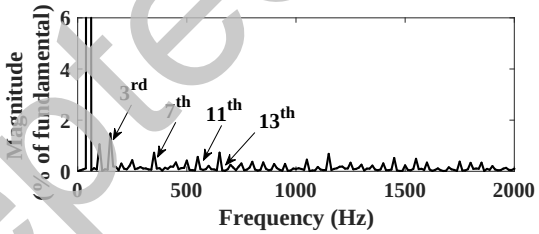

(b) Measured spectrum of (i_{sa}) using the conventional control structure.

Fig. 17: Case 1: frequency analysis of the current in case of 3% unbalanced grid voltage using the conventional and proposed control schemes.

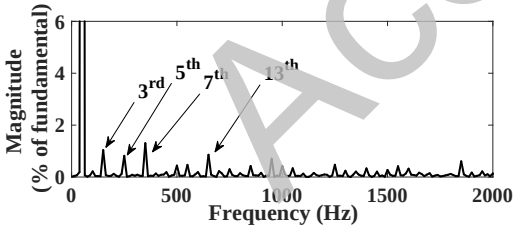

(a) Measured spectrum of (i_{sa}) using the proposed control structure.

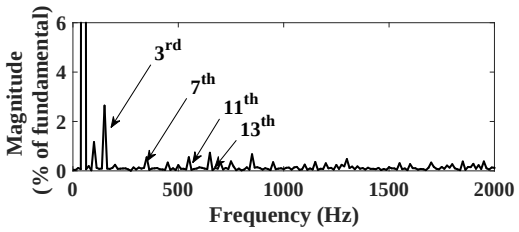

(b) Measured spectrum of (i_{sa}) using the conventional control structure.

Fig. 18: Case 2: frequency analysis of the current in case of 5% unbalanced grid voltage using the conventional and proposed control schemes.

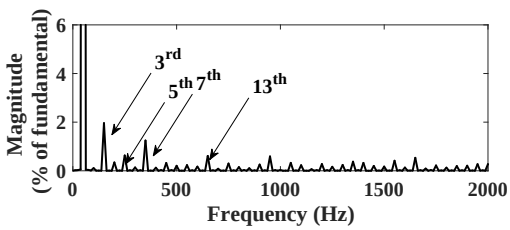

(a) Measured spectrum of (i_{sa}) using the proposed control structure.

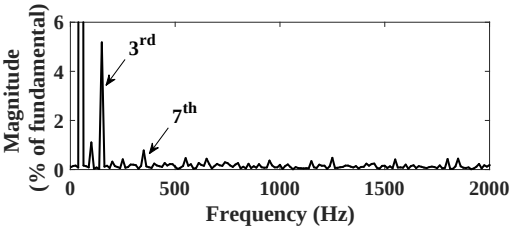

(b) Measured spectrum of (i_{sa}) using the conventional control structure.

Fig. 19: Case 3: frequency analysis of the current in case of 10% unbalanced grid voltage using the conventional and proposed control schemes.

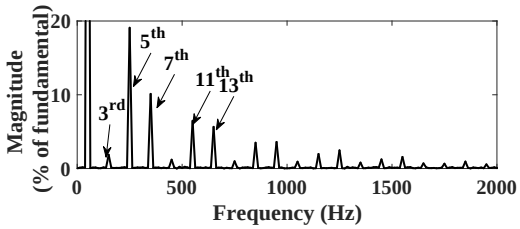

(a) Measured spectrum of (i_{sa}) in the case of 3% unbalance voltage.

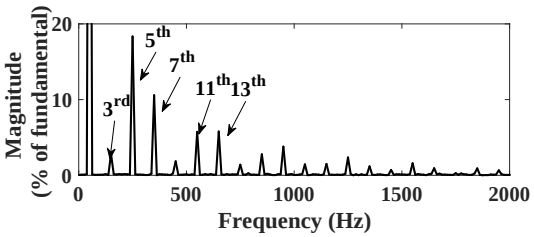

(b) Measured spectrum of (i_{sa}) in the case of 5% unbalance voltage.

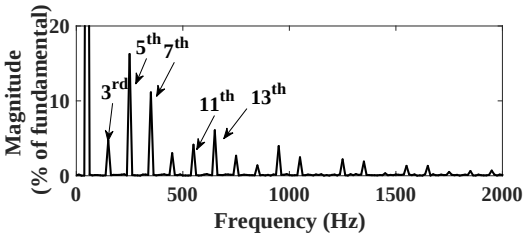

(c) Measured spectrum of (i_{sa}) in the case of 10% unbalance voltage.

Fig. 20: Frequency analysis of the current in case of 3%, 5%, and 10% unbalanced grid voltages where the SAPF is deactivated.

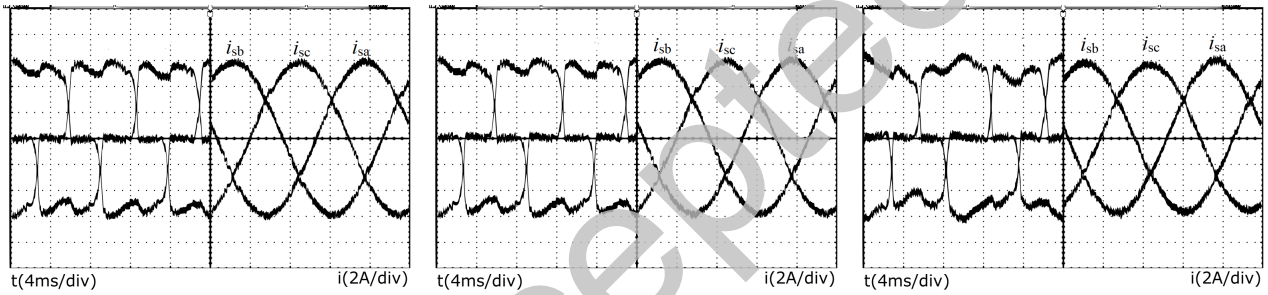

(a) 3% grid voltage unbalance (b) 5% grid voltage unbalance (c) 10% grid voltage unbalance

Fig. 21: Experimental results: harmonics and unbalance compensation for the proposed control structure in three different cases. (a) compensation in case of 3 % grid voltage unbalance; (b) compensation in case of 5 % grid voltage unbalance; and (c) compensation in case of 10 % grid voltage unbalance.

Table 2 Characteristics of the conventional and proposed control structures.

	SVPWM	Modulated MPC (M^2PC) proposed in [26]	Convetional MPC introduced in [26]	Proposed FCS-MPC
Harmonic extraction method (HEM)	DQ	PQ	PQ	DQ
Number of sensors needed by HEM	6	6	6	6
DC-link voltage regulator	PI	PI	PI	Without PI
THDi_s @6A up to 40th harmonics (balanced voltages)*	6.4%	N/A	N/A	6.7%
THDi_s @10A up to 40th harmonics (balanced voltages)	5.6%	6%	7%	5.1%
THDi_s @15A up to 40th harmonics (balanced voltages)	4.3%	N/A	N/A	3.6%
Sampling frequency (f_s)	20 kHz	20 kHz	50 kHz	50 kHz
Switching frequency (f_{sw})	10 kHz	N/A	N/A	Average = 10 kHz
Delay compansation (experemiental)	Yes	Yes	Yes	Yes
Cost Function	Three objectives	Three objectives	Three objectives	One objective
Numerical implementation	Transformations, Filtering, Tuning control	Transformations, Filtering, Tuning control	Transformations, Filtering, Tuning control	Transformations, Filtering
Number of transformations	3	3	3	4
Control bandwidth	Low	High	High	High
DC ripple	0.14%	<0.7%	<0.7%	0.08%
V_{dc}	700 V	700 V	700 V	700 V
L_f	5 mH	4.75 mH	4.75 mH	5 mH
Rated power for steady-state test	5 kW	5 kW	5 kW	5 kW
Rated power for transient test	from 5 kW to 8 kW	from 2.5 kW to 5 kW	from 2.5 kW to 5 kW	from 5 kW to 8 kW
Rated power for transient test (%)	From 33% to 53% of the full load (FL)	50% to 100% of the FL	50% to 100% of the FL	33% to 53% of the FL
Transient response time	Fast	Fast	Fast	Very fast

* THD$_i$ has been calculated from the experimental results.

7 References

1 S. P. Litran, P. Salmeron, J. R. Vazquez, R. S. Herrera, and A. Perez, "Control strategy for hybrid power filter to compensate unbalanced and non-linear, three-phase loads," *2009 13th European Conference on Power Electronics and Applications*, pp. 1–10, Sep. 2009.

2 K. Antoniewicz and M. Jasinski, "Experimental comparison of hysteresis based control and finite control state set model predictive control of shunt active power filter," *2015 Selected Problems of Electrical Engineering and Electronics (WZEE)*, pp. 1–6, Sep. 2015.

3 H. Afghoul and F. Krim, "Comparison between pi and fuzzy dpc control of a shunt active power filter," *2012 IEEE International Energy Conference and Exhibition (ENERGYCON)*, pp. 146–151, Sep. 2012.

4 A. Renault, M. Rivera, J. Rodas, L. Comparatore, J. Pacher, and R. Gregor, "Modulated model predictive current control for h-bridge two-level single phase active power filters statcom," *2017 12th IEEE Conference on Industrial Electronics and Applications (ICIEA)*, pp. 355–359, June 2017.

5 Y. Hoon, M. A. Mohd Radzi, M. K. Hassan, and N. F. Mailah, "Control algorithms of shunt active power filter for harmonics mitigation: A review," *Energies*, vol. 10, no. 12, 2017.

6 R. Rabbeni, L. Tarisciotti, A. Gaeta, A. Formentini, P. Zanchetta, M. Pucci, M. Degano, and M. Rivera, "Finite states modulated model predictive control for active power filtering systems," *2015 IEEE Energy Conversion Congress and Exposition (ECCE)*, pp. 1556–1562, Sep. 2015.

7 K. H. Kwan, Y. S. Png, Y. C. Chu, and P. L. So, "Model predictive control of unified power quality conditioner for power quality improvement," *2007 IEEE International Conference on Control Applications*, pp. 916–921, Oct 2007.

8 S. Rahmani, A. Hamadi, K. Al-Haddad, and L. A. Dessaint, "A combination of shunt hybrid power filter and thyristor-controlled reactor for power quality," *IEEE Transactions on Industrial Electronics*, vol. 61, pp. 2152–2164, May 2014.

9 V. K. Gonuguntala, A. Frobel, and R. Vick, "Performance analysis of finite control set model predictive controlled active harmonic filter," *2018 18th International Conference on Harmonics and Quality of Power (ICHQP)*, pp. 1–6, May 2018.

10 S. C. Ferreira, R. B. Gonzatti, R. R. Pereira, C. H. da Silva, L. E. B. da Silva, and G. Lambert-Torres, "Finite control set model predictive control for dynamic reactive power compensation with hybrid active power filters," *IEEE Transactions on Industrial Electronics*, vol. 65, pp. 2608–2617, March 2018.

11 H. Akagi, E. H. Watanabe, and M. Aredes, *Instantaneous power theory and applications to power conditioning*. John Wiley & Sons, 2017.

12 L. Malesani, P. Mattavelli, and S. Buso, "Robust dead-beat current control for pwm rectifiers and active filters," *IEEE Transactions on Industry Applications*, vol. 35, pp. 613–620, May 1999.

13 H. Soltani, P. Davari, F. Blaabjerg, and F. Zare, "Harmonic distortion performance of multi three-phase scr-fed drive systems with controlled dc-link current under unbalanced grid," *IECON 2017 - 43rd Annual Conference of the IEEE Industrial Electronics Society*, pp. 1210–1214, Oct 2017.

14 D. Kumar, P. Davari, F. Zare, and F. Blaabjerg, "Analysis of three-phase rectifier systems with controlled dc-link current under unbalanced grids," *2017 IEEE Applied Power Electronics Conference and Exposition (APEC)*, pp. 2179–2186, March 2017.

15 Tianqu Hao, Li Ran, Zheng Zeng, and Wei Lai, "Fast extraction of positive and negative sequence voltage components for inverter control," *8th IET International Conference on Power Electronics, Machines and Drives (PEMD 2016)*, pp. 1–6, April 2016.

16 A. Camacho, M. Castilla, J. Miret, L. G. de Vicuna, and R. Guzman, "Positive and negative sequence control strategies to maximize the voltage support in resistive inductive grids during grid faults," *IEEE Transactions on Power Electronics*, vol. 33, pp. 5362–5373, June 2018.

17 L. Tarisciotti, A. Formentini, A. Gaeta, M. Degano, P. Zanchetta, R. Rabbeni, and M. Pucci, "Model predictive control for shunt active filters with fixed switching frequency," *IEEE Transactions on Industry Applications*, vol. 53, pp. 296–304, Jan 2017.

18 C. Hu, Y. Wang, S. Luo, and H. Wang, "Voltage control strategy of islanded three-phase voltage source converter under unbalanced loads based on disturbance observer," *2018 21st International Conference on Electrical Machines and Systems (ICEMS)*, pp. 2199–2204, Oct 2018.

19 M. Rane and S. Wagh, "Mitigation of harmonics and unbalanced source voltage condition in standalone microgrid: positive sequence component and dynamic phasor based compensator with real-time approach," *Heliyon*, vol. 5, no. 2, p. e01178, 2019.

20 H. Young and J. Rodriguez, "Comparison of finite-control-set model predictive control versus a svm-based linear controller," *2013 15th European Conference on Power Electronics and Applications (EPE)*, pp. 1–8, Sep. 2013.

21 M. Aguirre, S. Kouro, C. A. Rojas, J. Rodriguez, and J. I. Leon, "Switching frequency regulation for fcs-mpc based on a period control approach," *IEEE Trans. on Ind. Electron.*, vol. 65, pp. 5764–5773, July 2018.

22 J. Rodriguez, J. Pontt, C. Silva, P. Cortes, U. Amman, and S. Rees, "Predictive current control of a voltage source inverter," *2004 IEEE 35th Annual Power Electronics Specialists Conference (IEEE Cat. No.04CH37551)*, vol. 3, pp. 2192–2196 Vol.3, June 2004.

23 P. Cortes, G. Ortiz, J. I. Yuz, J. Rodriguez, S. Vazquez, and L. G. Franquelo, "Model Predictive Control of an Inverter With Output LC Filter for UPS Applications," *IEEE Trans. on Ind. Electron.*, vol. 56, pp. 1875–1883, June 2009.

24 P. Cortes, J. Rodriguez, S. Vazquez, and L. G. Franquelo, "Predictive control of a three-phase UPS inverter using two steps prediction horizon," *ICIT, 2010 IEEE Int. Conf. on*, pp. 1283–1288, March 2010.

25 M. Tomlinson, H. d. T. Mouton, R. Kennel, and P. Stolze, "A fixed switching frequency scheme for finite-control-set model predictive controlâĂŤconcept and algorithm," *IEEE Transactions on Industrial Electronics*, vol. 63, pp. 7662–7670, Dec 2016.

26 L. Tarisciotti, A. Formentini, A. Gaeta, M. Degano, P. Zanchetta, R. Rabbeni, and M. Pucci, "Model predictive control for shunt active filters with fixed switching frequency," *IEEE Transactions on Industry Applications*, vol. 53, pp. 296–304, Jan 2017.

27 Wang Xiao-gang, Xie Yun-xiang, and Shuai Ding-xin, "Simplified model predictive control for a shunt active power filter," *2008 IEEE Power Electronics Specialists Conference*, pp. 3279–3283, June 2008.

28 R. Panigrahi, B. Subudhi, and P. C. Panda, "Model predictive-based shunt active power filter with a new reference current estimation strategy," *IET Power Electronics*, vol. 8, no. 2, pp. 221–233, 2015.

29 S. Biricik, O. C. Ozerdem, S. Redif, and M. O. I. Kmail, "Performance improvement of active power filters based on p-q and d-q control methods under non-ideal supply voltage conditions," *2011 7th International Conference on Electrical and Electronics Engineering (ELECO)*, pp. I–312–I–316, Dec 2011.

30 S. M. I. Rahman, M. A. Abdulla Samy, and S. Saha, "C-code implementation of a shunt active power filter based on finite set model predictive control," *2019 International Conference on Robotics,Electrical and Signal Processing Techniques (ICREST)*, pp. 359–363, Jan 2019.

31 A. Al-Othman, M. AlSharidah, N. A. Ahmed, B. N. Alajmi, *et al.*, "Model predictive control for shunt active power filter in synchronous reference frame," *J Electr Eng Technol*, vol. 11, pp. 1921–718, 2016.

32 Y. Zhang, J. Liu, and S. Fan, "On the inherent relationship between finite control set model predictive control and svm-based deadbeat control for power converters," *2017 IEEE Energy Conversion Congress and Exposition (ECCE)*, pp. 4628–4633, Oct 2017.

33 P. Cortes, J. Rodriguez, C. Silva, and A. Flores, "Delay Compensation in Model Predictive Current Control of a Three-Phase Inverter," *IEEE Trans. on Ind. Electron.*, vol. 59, pp. 1323–1325, Feb 2012.